Hysteresis-Dependent Adsorption-Desorption Cycles: Generalization for Isothermal Conditions

Pavol Rajniak and Ralph T. Yang
Dept. of Chemical Engineering, State University of New York at Buffalo, Buffalo, NY 14260

Hysteresis-dependent adsorption-desorption equilibrium cycles are measured for the systems water vapor-silica gel at 25°C. Various and distinct types of equilibrium cycles are observed, depending on the relative positions of the limiting partial pressures with respect to the closure points of the main hysteresis loop as well as the history of the cycle. Hysteresis-dependent cycles are classified accordingly. The simple theoretical model based on the network pore blocking theory for predicting primary and secondary adsorption and desorption isotherms (Rajniak and Yang, 1993) is extended for predicting isotherms of higher orders and equilibrium cycles of all types. Only primary adsorption and desorption isotherms are needed for the predictions. Furthermore, there exists an infinite number of equilibrium cycles between any two partial pressures within the main hysteresis loop; the exact path of the cycle depends on the history before the cycle is initiated—it is memory-dependent.

Introduction

Cyclic adsorption-desorption processes are widely employed in separation and purification of gases. In particular, the cyclic pressure swing adsorption process (PSA) has an increasing number of applications. One of the first and most important applications of the PSA process is the drying of air and industrial gases (Yang, 1987). A preferred sorbent for drying is silica gel. The hysteresis effects for equilibria of condensable adsorptives on silica gel are well known (Gregg and Sing, 1982), and particularly for water the hysteresis was first observed almost a century ago (Van Bemmelen, 1897). Many experimental and theoretical studies have been reported on the hysteresis phenomenon. Most of them have been discussed in our previous article (Rajniak and Yang, 1993). Of particular interest to this study is the review of Everett (1967) and the studies of Mayagoitia and coworkers (Mayagoitia et al., 1988a, b). Hysteresis has also been considered in modeling once-through fixed-bed desorption by Ritter and Yang (1991). In their work, the effect of hysteresis was studied by comparing the fixed-bed desorption along the adsorption branch of the isotherm (without hysteresis) with that along the desorption branch (with hysteresis). The initial conditions of the bed were chosen such that desorption along any secondary (scanning) desorption curves was avoided. The equilibrium theory of that work (Ritter and Yang, 1991), although quite general, applied rigorously only to the case of elution of a uniformly saturated bed of a single dilute adsorbate with an inert carrier gas. The extension of their approach to the cases of desorption of a nonuniformly saturated bed called for another method. Recently, Rajniak and Yang (1993) proposed a simple model for the evaluation and prediction of hysteresis-dependent sorption data. For *a priori* prediction of the secondary (scanning) adsorption and desorption curves starting, respectively, from the primary (boundary) desorption and adsorption curves, only the primary adsorption and primary desorption data are needed. The proposed method was applied to the experimental sorption data of water vapor on silica gel. A simple sequential evaluation procedure was used to find the parameters of primary isotherms and the position of their intersections. The usefulness of the model was supported by its agreement with experimental data. The model used in our recent work (Rajniak and Yang, 1993) was based on the use of pore-blocking interpretation of hysteresis in an interconnected network of pores originally proposed by Mason (1983, 1988) and further extended by Parlar and Yortsos (1988, 1989). For the prediction of cyclic adsorption-desorption processes with the presence of hysteresis effects, further important characteristics of hysteresis phenomena, that is, higher-order scanning curves and cyclic loops, need to be considered. Various typical sets of ascending and

Correspondence concerning this article should be addressed to R. T. Yang.
Present address of P. Rajniak: Department of Chemical Engineering, Slovak Technical University, 812 37 Bratislava, Slovakia.

descending scanning curves forming cyclic and spiral paths inside the main hysteresis loop are reviewed excellently by Everett (1967).

The first objective of this study was to provide sets of experimental cyclic adsorption-desorption data at various limiting relative pressures both inside and outside the main hysteresis loop for the previously studied system of water vapor on silica gel. The second objective was to extend the pore blocking theory (Mason, 1983, 1988) for the prediction of higher-order (secondary, tertiary, and so on) adsorption-desorption processes starting from various points inside the main hysteresis loop and to develop general relations for the prediction of any isothermal hysteresis-dependent equilibrium cyclic processes.

Theoretical Considerations

Equilibrium hysteresis-dependent cycles

We consider equilibrium, cyclic adsorption-desorption processes in a porous adsorbent. Figure 1 shows typical hysteresis-dependent equilibrium cyclic processes starting from a clean particle (at point S). During primary adsorption, the porous adsorbent initially free of adsorbate is exposed to a vapor mixture containing one adsorptive and inert. When the equilibrium amount adsorbed on the primary adsorption curve at point 6 is reached, the process is reversed. The partial pressure of the adsorptive is decreased, and adsorbent pores are emptied during primary desorption. For the system with hysteresis, the equilibrium amount adsorbed during the primary desorption at any partial pressure between points U and L is greater as it was during primary adsorption. The primary desorption can terminate at point 5. Point 5 is termed reversal point where the decreasing relative vapor pressure is reversed. In the next steps of the process, the relative pressure is increased, and the resulting equilibrium curve is termed secondary adsorption and lies between the primary adsorption and primary desorption curves. All three curves intersect at point U, the upper closure point of the hysteresis loop. For relative pressures greater than x^U, all three curves coincide and the process is reversible. The cyclic process can be repeated and the corresponding equilibrium path is 6 - U - 5 - U - 6.

Classification of equilibrium cycles

The cyclic process analyzed above represents only one of the possible paths, and many other paths are possible depending on the positions of the limiting (reversal) points of the process. Figures 1-3 show various hysteresis-dependent cycles between two fixed relative pressures.

In the following we introduce a classification of hysteresis-dependent equilibrium cycles. To simplify the classification, only cycles operating between two fixed relative pressures x_{j-1} and x_j are considered. Generally, the relative pressures x_{j-1}, x_j differ from the relative pressure x_s at the starting point of the adsorption-desorption process (point S). The term hysteresis-dependent cycle applies when at least one of the relative pressures, x_{j-1} and x_j, lies between the limiting pressures of the main hysteresis loop (bounded by the closure points x^L and x^U). We propose the following classification:

1. Cycles starting with adsorption from point S for which $0 \le x_s < x^L$ (such as adsorption on a clean particle): Cycles C1, C2, and C3 in Figure 1.

2. Cycles starting with desorption from point S for which $x^U < x_s \le 1$ (such as desorption from a nearly saturated bed): Cycles C1, C4, and C3 in Figure 2.

3. Cycles starting with desorption from point S for which $x^L \le x_s \le x^U$ (such as desorption from a partially saturated particle): Cycles C1, C5, and C3 in Figure 3.

Cycle C1 operates between limiting points 1 and 2 and the corresponding equilibrium path is S - {1 - L - 2 - L- 1} during the cyclic process starting from a clean particle (Figure 1), or

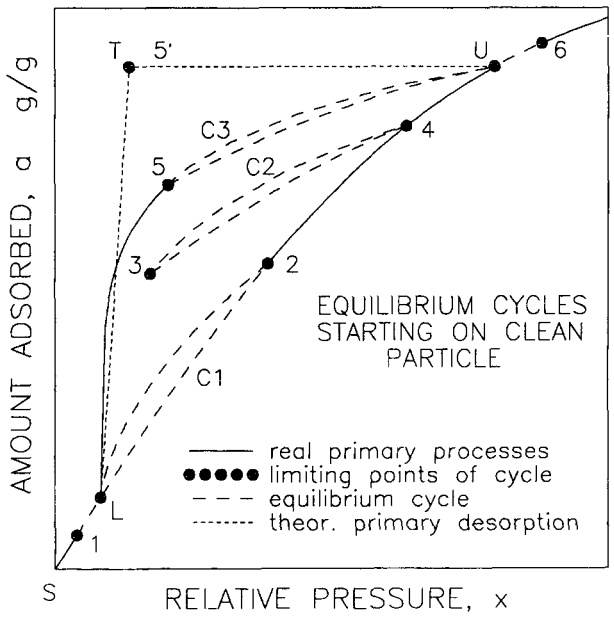

Figure 1. Classification of adsorption-desorption hysteresis-dependent cycles starting from clean particle.

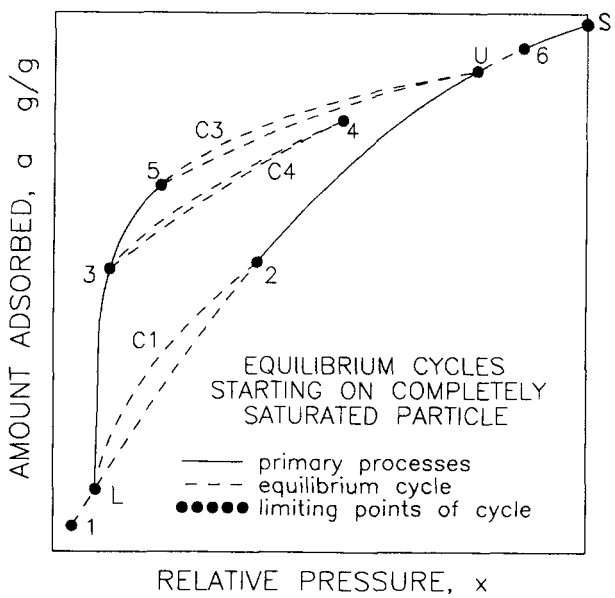

Figure 2. Classification of adsorption-desorption hysteresis-dependent cycles starting from completely saturated particle.

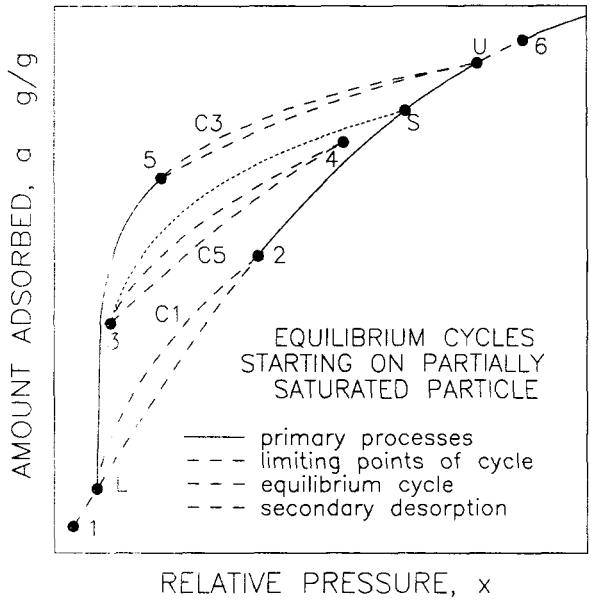

Figure 3. Classification of adsorption-desorption hysteresis-dependent cycles starting from partially saturated particle.

the path is S - U - L - {1 - L - 2 - L - 1} during the cyclic process starting from a saturated particle (Figure 2), or the path is S - 3 - L - {1 - L - 2 - L - 1} during the cyclic process started from a partially saturated particle (Figure 3).

Cycle C2 operates between limiting points 3 and 4 with the equilibrium path S - L - {4 - 3 - 4} during the cyclic process starting from a clean particle (Figure 1).

Cycle C3 operates between limiting points 5 and 6 with the equilibrium path S - L - U - {6 - U - 5 - U - 6} during the cyclic process starting from a clean particle (Figure 1), or the path is S - {6 - U - 5 - U - 6} during the process starting from a saturated particle (Figure 2), or the path is S - U - {6 - U - 5 - U - 6} during the process starting from a partially saturated particle (Figure 3).

The existence of cycles C3 requires the following clarification. Earlier we introduced curve types termed as primary (boundary) adsorption curve {0 - 1 - 2 - 4 - U - 6} and primary (boundary) desorption curve {6 - U - 5 - L - 1 - 0}. Also one of the secondary adsorption curves was shown in Figure 1 (curve 5 - U). This secondary adsorption curve commences at point 5 on the primary desorption curve, where the relative pressure $x^5 > x^T$ and x^T is the relative pressure corresponding to point T (see Figure 1), the primary desorption threshold. The position of this threshold point is important from both theoretical and experimental points of view. Using the percolation model for the adsorption-desorption phenomena with hysteresis, the initial part of the desorption branch (between points U and T) should be a horizontal line. Along this desorption branch there is theoretically no desorption. Desorption should begin only at point T, the percolation threshold of the primary desorption, when there is sufficient number of vapor connections in the porous network and the desorption from the bulk of the adsorbent can start. This theoretical model is not completely fulfilled for real experimental data, because the initial part of the primary desorption branch is not horizontal and desorption does occur. There are various explanations for this fact: decompression of the liquid phase (Mason, 1988; Seaton, 1991), nucleation effects (Parlar and Yortsos, 1989), vaporization via surface clusters (Liu et al., 1992), or desorption from the largest mesopores, emerging directly at the external surface (Neimark, 1991). Moreover, the experimental desorption-adsorption cycles are not reversible along the boundary desorption curve, but along narrow hysteresis loops that exist in this domain (Mason, 1988; this work), that is, between points T and U. It is difficult to discern which of the possible effects mentioned above plays the most important role and causes the irreversibility of the primary desorption curve in this domain. We use the same theoretical model for prediction of secondary adsorption branches of cycles C3 starting from any point on the primary desorption isotherm, below as well as above the threshold point T.

Cycle C4 operates between limiting points 3 and 4 with the equilibrium path S - U - {3 - 4 - 3} during the process starting from a saturated particle (Figure 2).

Cycle C5 operates between limiting points 3 and 4 with the equilibrium path S - {3 - 4 - 3} during the process starting from S below point U (Figure 3).

History dependence of cycle path

For cycles C2, C4, and C5 operating between any points $j-1$ and j with relative pressures x_{j-1} and x_j within the closure points L and U, the resulting equilibrium path will depend on the "history" of the process, on the position of the starting point S. An infinite number of different equilibrium paths can be obtained depending on the position of point S in Figure 4. However, if either one of the two points $j-1$ and j lies outside the closure points, L and U, the resulting cyclic loop is of type C1 or C3.

Figure 5 shows another equilibrium cycle operating between points 3 and 4 inside the main hysteresis loop. The corresponding equilibrium path is S - U - 1 - {2 - 3 - 4 = 2}. This

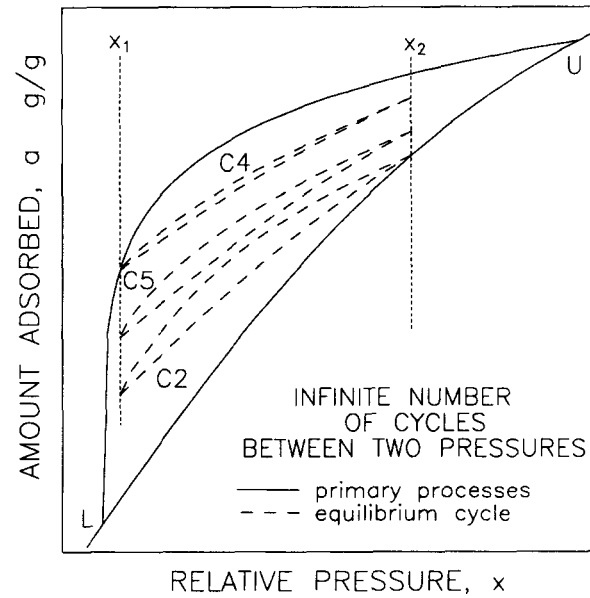

Figure 4. Infinite number of possible equilibrium cycles between the same two pressures depending on the history of the cyclic process.

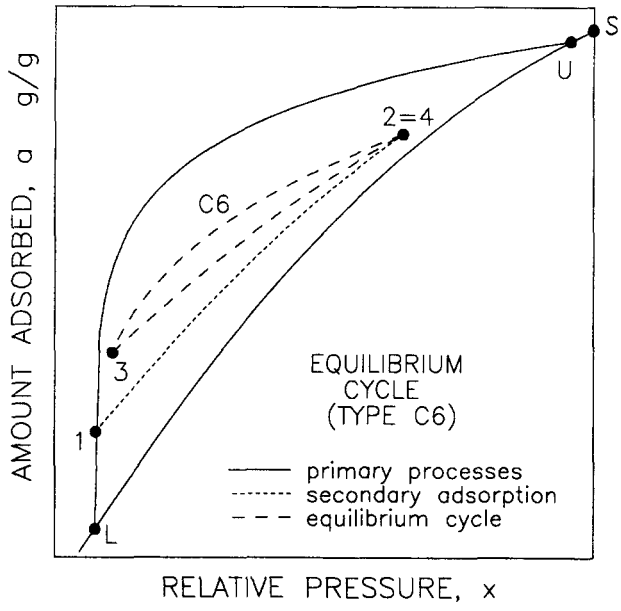

Figure 5. Equilibrium cycle type C6 operating between points 3 and 4, starting from completely saturated particle.

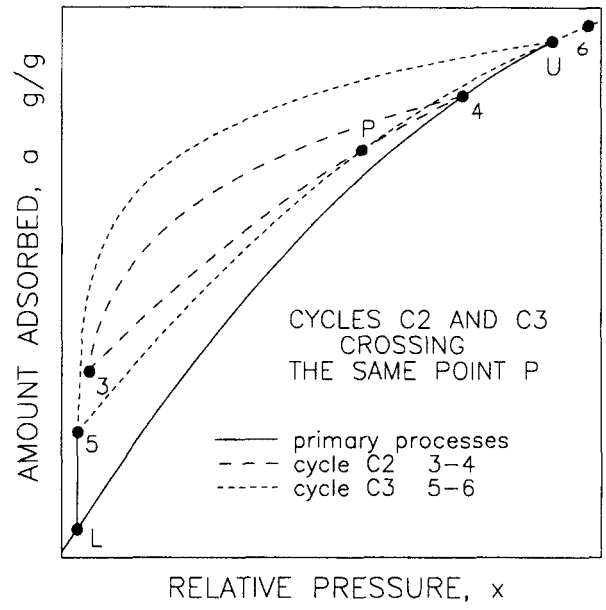

Figure 6. Two different pathways crossing the same point P depending on the history of the adsorption-desorption process.

type of cycle (C6 in Figure 5) is not included in the basic classification, because it operates between three different relative pressures x_1, $x_2 = x_4$ and x_3. However, this cycle demonstrates the variety of possible equilibrium paths inside the main hysteresis loop.

Another interesting feature of the hysteresis-dependent equilibrium process is shown in Figure 6. There exist two crossover loops intersecting at two points, one of which is P. The path at point P will depend on the "history" of the system before it reaches point P (see also cycles C2 and C3 in Figure 1). This shows that the loops depend on memory.

For the theoretical prediction of various equilibrium cycles discussed above, a generalization and extension of Mason's model (1983, 1988) is needed, because Mason's original model was developed only for the primary and secondary adsorption and desorption processes.

The theoretical principles of the mathematical model are discussed in detail elsewhere (Mason, 1988; Rajniak and Yang, 1993), and therefore we present only the main assumptions and the basic relations of the model:

(1) A porous material consists of bonds and sites. The average number of bonds connecting a site with neighboring sites is connectivity C.

(2) The pore structure model used for the interconnectedness of the pore network is the Bethe tree.

(3) Capillary condensation phenomena control the sorption processes in the whole range of the hysteresis loop, and the secondary issues of surface adsorption in this domain are neglected.

(4) For description of the primary adsorption curve we can use any suitable adsorption isotherm such as Dubinin-Astakhov (DA) equation:

$$a_A = a_{mA} \exp\left[-\left(K_A \ln \frac{1}{x} \right)^{n_A} \right] \tag{1a}$$

used in our previous work (Rajniak and Yang, 1993), or a two-site Dubinin-Radushkevich (DR2) expression:

$$a_A = a_{mA1} \exp\left[-\left(K_{A1} \ln \frac{1}{x} \right)^2 \right] + a_{mA2} \exp\left[-\left(K_{A2} \ln \frac{1}{x} \right)^2 \right] \tag{1b}$$

which is particularly suitable for the experimental system silica gel-water vapor (Van den Bulck, 1990; Park and Knaebel, 1992).

(5) For theoretical calculation of the primary and secondary desorption curves, the combination of the pore blocking effects and the percolation theory yields the following set of relations:

For the fraction of pores filled by capillary condensation, S, we have (neglecting surface adsorption in the hysteresis domain):

$$S = \frac{a^t - a^L}{a^U - a^L} \tag{2}$$

where a^t is the *theoretical* amount adsorbed during any sorption process in the hysteresis domain.

For the fraction of pores filled during primary or secondary desorption starting from the point j on the primary adsorption curve we have the following theoretical results originally derived by Mason (1988):

$$S_d = q_j \left\{ q_j \left[(1-u) + u \frac{p}{p_j} \right] + (1-q_j) \frac{p}{p_j} \right\}^C \tag{3}$$

$$(1-u) = \left\{ q_j \left[(1-u) + u \frac{p}{p_j} \right] + (1-q_j) \frac{p}{p_j} \right\}^{C-1} \tag{4}$$

where the subscript $d=D$ stands for the primary desorption ($q_j=1, p_j=1$) and $d=SD$ for the secondary desorption ($q_j<1$, $p_j<1$). In Eqs. 3 and 4 the probabilities p and q are defined by:

$$p=\int_0^{r_p} f(r)dr \tag{5}$$

$$q=\int_0^{r_q} g(r)dr \tag{6}$$

where functions $f(r)$ and $g(r)$ represent the pore bond (window) size distribution function and the pore site size distribution function, respectively, r is the characteristic dimension of the bond or of the site which can be related to relative pressure via Kelvin equation for capillary condensation:

$$r=-\frac{b(T)}{\ln x} \tag{7}$$

where coefficient b is a function of temperature. The probabilities p and q are related through connectivity C:

$$p^C=q \tag{8}$$

where C is defined as the average number of bonds per pore (site). The variable u in Eqs. 3 and 4 gives the probability that at a particular value of p an initially filled bond into a site now has an emptied neighbor and so has a connection to the vapor. For the starting point of the secondary desorption, $x=x_j$, $q=q_j$, $p=p_j$ and $u=0$. For the primary adsorption, the following simple relation exists between q and a_A, amount adsorbed, and S_A, fraction of pores filled:

$$S_A=q=\frac{a_A-a^L}{a^U-a^L} \tag{9}$$

Calculation for the amount adsorbed during primary desorption (for $q_j=1$) or during secondary desorption ($0<q_j<1$) requires an iteration procedure. Combining Eqs. 2-4, 8 and 9 we get after several manipulations the following result relating the amount adsorbed during primary adsorption, a_A, to the theoretical adsorbed amount during primary desorption, a'_D (for $a_{Aj}=a^U$) or during secondary desorption, a'_{SD} (for $a_{Aj}<a^U$)

$$a_A=a^L+(a_{Aj}-a^L)\left[\frac{e_j^{(C-1)/C^2}-f_j\,e_j^{(C-1)/C}}{1-f_j\,e_j^{(C-1)/C}}\right]^C \tag{10}$$

where $$e_j=\frac{a'_d-a^L}{a_{Aj}-a^L} \quad \text{and} \quad f_j=\frac{a_{Aj}-a^L}{a^U-a^L}$$

Expressing a_4 via Eq. 1a or 1b we have the implicit relation between the relative pressure x and the theoretical amount adsorbed during desorption, a'_d (subscript $d=D$ stands for primary desorption and subscript $d=SD$ for secondary desorption). Equations 5-7 are not employed for the calculation of the amount adsorbed during primary or secondary desorption process, respectively, but they are useful for the evaluation of the pore bond size or pore site size distribution functions, respectively (Mason, 1988).

(6) For prediction of the secondary adsorption isotherm starting from any point $j-1=\{x_{j-1}, a_{D,j-1}\}$ on the primary desorption isotherm, the following relation was derived (Mason, 1988) for the fraction of pores filled during secondary adsorption, S_{SA}:

$$S_{SA}=S_{j-1}+(1-S_{j-1})\frac{q-q_{j-1}}{1-q_{j-1}} \tag{11}$$

which can be rewritten (Rajniak and Yang, 1993; see also Figure 1) for the amount adsorbed a_{SA}:

$$a_{SA}=a^U\left(\frac{a_{D,j-1}-a_{A,j-1}}{a^U-a_{A,j-1}}\right)+\left(\frac{a^U-a_{D,j-1}}{a^U-a_{A,j-1}}\right)a_A \tag{12}$$

Generalization of pore-blocking model for higher-order processes

Equations 1a (or 1b), 10, and 12 represent the final set of expressions for the theoretical prediction of the primary processes and for the prediction of the secondary processes starting from the primary curves. For prediction of the secondary processes starting from any point inside the main hysteresis loop and for prediction of higher-order processes (tertiary, quarternary, and so on), extension of Mason's model follows.

In Figure 7 a general spiral path is shown. During the cyclic equilibrium process starting from a clean particle (at point 1), the adsorbent is first partially filled by capillary condensation during primary adsorption (process 1 - 2). Then the process is reversed at point 2 on the primary adsorption curve before reaching the upper closure point U and the secondary desorption (process 2 - L) starts. The process is again reversed at point 3 inside the main hysteresis loop before reaching the lower closure point L and secondary adsorption (process 3 -

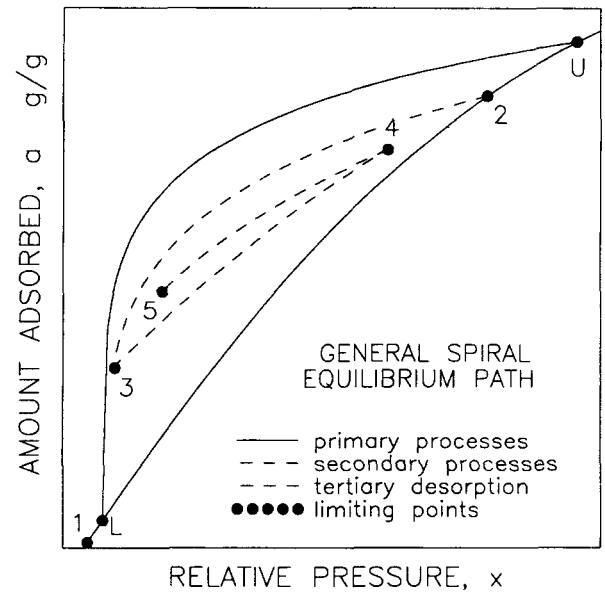

Figure 7. General spiral equilibrium path: higher-order cycles.

2) begins. The process is again reversed at point 4 inside the main hysteresis loop before reaching point 2 and tertiary desorption (process 4 - 3) commences, which is stopped at point 5. The process may continue. The predictive relations for the *primary adsorption* and for the *secondary desorption* have been discussed above.

The derivation for the respective *secondary adsorption* isotherm between points 3 and 2 is analogous to the procedure reported by Mason (1988):

At the turning point 2 on the primary adsorption curve the fraction of pores filled is S_2 and the corresponding probability is q_2, and at the turning point 3 the corresponding values are S_3 and q_3. The fraction emptied during the secondary desorption is simply $S_2 - S_3$. We consider a general point on the secondary adsorption isotherm given by the probability q and the fraction of pores filled S_a. The probability of an initially empty pore being refilled at q is given by $(q - q_3)/(q_2 - q_3)$ and this gives the fraction of the emptied pores being refilled at q. The fraction S filled at q is thus the sum of the fraction S_3 that was never emptied plus a fraction $(q - q_3)/(q_2 - q_3)$ of that which was emptied $(S_2 - S_3)$ and is now refilled:

$$S_a = S_3 + (S_2 - S_3)\,\frac{q - q_3}{q_2 - q_3} \tag{13}$$

The secondary adsorption process described by Eq. 13 operates between points 3 and 2 and can intersect the primary adsorption curve at point 2 (for $q = q_2$, we get $S = S_2$). During the cyclic process shown in Figure 7 the secondary adsorption process is reversed at point 4 where $q = q_4$ and $S_a = S_4$, computed from Eq. 13.

The *tertiary desorption* process between points 4 and 3 can be calculated as follows:

At the turning point 4 on the secondary adsorption curve the fraction of pores filled is:

$$S_4 = S_3 + (S_2 - S_3)\,\frac{q_4 - q_3}{q_2 - q_3} \tag{14}$$

computed via Eq. 13. The corresponding probabilities are q_4 and $p_4 = q_4^C$. At any general point on the tertiary desorption curve, let the fraction of pores filled be S_d and the corresponding probabilities be p and q. At some stage during desorption, the probability that an initially filled bond into a cell (site) that now has an emptied neighbor is u (at the start of the tertiary desorption at point 4, $u = 0$). The probability of such bond not passing a meniscus is given by $(p - p_3)/(p_4 - p_3)$. This normalized probability is equal to 1 for $p = p_4$ (start of the tertiary desorption) and is equal to 0 for $p = p_3$ (end of the tertiary desorption). A cell (site) that is initially filled has a probability $(q_4 - q_3)/(q_2 - q_3)$ of having a filled neighbor at the end of a bond, and a probability $1 - (q_4 - q_3)/(q_2 - q_3)$ of having an emptied neighbor at the end of the bond. At a subsequent value of $p < p_4$, the probability that a bond has an emptied neighbor is u and so the probability that the bond is still unconnected is $(1 - u)$. If the bond has an empty neighbor, then the probability that the meniscus does not pass is $(p - p_3)/(p_4 - p_3)$. So the probability that an initially filled pore has not emptied by a particular single bond is given by $(q_4 - q_3)/(q_2 - q_3)$, the probability that the neighbor was initially filled, multiplied by the sum of the probability that the bond has not become connected $(1 - u)$ and the probability that, if it has become connected (u), a meniscus does not pass $(p - p_3)/(p_4 - p_3)$, plus the probability $1 - (q_4 - q_3)/(q_2 - q_3) = (q_2 - q_4)/(q_2 - q_3)$, that the neighbor was initially empty, and the probability that a meniscus does not pass $(p - p_3)/(p_4 - p_3)$. If C-1 bonds around a filled cell (site) have not emptied then the remaining bond is not emptied. But this has probability $(1 - u)$ and in summary we get:

$$1 - u = \left\{\frac{q_4 - q_3}{q_2 - q_3}\left[1 - u + u\,\frac{p - p_3}{p_4 - p_3}\right] + \frac{q_2 - q_4}{q_2 - q_3}\,\frac{p - p_3}{p_4 - p_3}\right\}^{C-1} \tag{15}$$

The fraction of cells that remain filled is given by the fraction S_3 that was never emptied plus the fraction of those which can be emptied $(S_2 - S_3)$ multiplied by the probability $(q_4 - q_3)/(q_2 - q_3)$ that the cell was initially filled multiplied by the probability that all C links do not pass a meniscus:

$$S_d = S_3 + (S_2 - S_3)\,\frac{q_4 - q_3}{q_2 - q_3}\left\{\frac{q_4 - q_3}{q_2 - q_3}\left[1 - u + u\,\frac{p - p_3}{p_4 - p_3}\right] + \frac{q_2 - q_4}{q_2 - q_3}\,\frac{p - p_3}{p_4 - p_3}\right\}^{C} \tag{16}$$

The tertiary desorption process operates between points 4 and 3. At point 4 we get, for $u = 0$ and $p = p_4$, $S_d = S_4$, which is equivalent to Eq. 14, and at point 3, for $u = 1$ and $p = p_3$, we get $S_d = S_3$. Any further desorption process (for $p < p_3$) continues along the curve 2 - 3 - L and is predicted by Eqs. 3 and 4 for the preceding secondary desorption process.

Reversing the tertiary desorption at the point 5 before reaching point 3, the *tertiary adsorption* process commences and is described by:

$$S_a = S_5 + (S_4 - S_5)\,\frac{q - q_5}{q_4 - q_5} \tag{17}$$

In the same manner, the theoretical relations for the next and further desorption and adsorption processes can be derived. The results can be written in the *general* form for any *adsorption* process (starting at the point $j - 1 = \{S_{j-1}, q_{j-1}\}$):

$$S_a = S_{j-1} + (S_{j-2} - S_{j-1})\,\frac{q - q_{j-1}}{q_{j-2} - q_{j-1}} \tag{18}$$

and the *general* form for the subsequent *desorption* process (starting at the point $j = \{S_j, q_j\}$ before reaching the point $j - 2 = \{S_{j-2}, q_{j-2}\}$)

$$S_d = S_{j-1} + (S_{j-2} - S_{j-1})\,\frac{q_j - q_{j-1}}{q_{j-2} - q_{j-1}}\left\{\frac{q_j - q_{j-1}}{q_{j-2} - q_{j-1}}\times\left[1 - u + u\,\frac{p - p_{j-1}}{p_j - p_{j-1}}\right] + \frac{q_{j-2} - q_j}{q_{j-2} - q_{j-1}}\,\frac{p - p_{j-1}}{p_j - p_{j-1}}\right\}^{C} \tag{19}$$

where

$$1-u=\left\{\frac{q_j-q_{j-1}}{q_{j-2}-q_{j-1}}\left[1-u+u\,\frac{p-p_{j-1}}{p_j-p_{j-1}}\right]+\frac{q_{j-2}-q_j}{q_{j-2}-q_{j-1}}\,\frac{p-p_{j-1}}{p_j-p_{j-1}}\right\}^C \quad (20)$$

Without loss of generality, we used the normalized probability u for each desorption process ($u=0$ at the start of the desorption process at point j and $u=1$ at the end of the desorption process at point $j-1$). Alternatively, we may replace u with $(u-u_j)/(u_{j-1}-u_j)$. Similar simplifications are not recommended for the probabilities p and q, because they are related to the partial pressure x and the amount adsorbed a_A via Eqs. 5-7 and 9.

From Eqs. 18-20, the predictive relations for any isothermal adsorption or desorption hysteresis-dependent process can be derived. The history of the process is necessary. For example, for the special case of primary adsorption process, we may imagine that the process starts after complete adsorption ($q_{j-2}=S_{j-2}=1$) followed by complete desorption ($q_{j-1}=S_{j-1}=0$). Introducing these values into Eq. 18 we get a relation equivalent to Eq. 9 for primary adsorption. Similarly, the predictive Eq. 11 for secondary adsorption is obtained by introducing $q_{j-2}=S_{j-2}=1$ and $q_{j-1}>0$ and $S_{j-1}>0$ into Eq. 18. On the other hand, the theoretical predictive equations, Eqs. 3 and 4, for the secondary desorption can be derived from Eqs. 19 and 20 by introducing $q_{j-2}=S_{j-2}=1$, $q_{j-1}=S_{j-1}=0$, $q_j>0$ and $S_j>0$. Obviously, by introducing also $q_j=S_j=1$, the solution is reduced to the theoretical expressions of Mason (1988) for primary desorption.

The general relation, Eq. 18, for the fraction of pores filled, S_a, can be rewritten to calculate the amount adsorbed, a_a. Using the definition relation (Eq. 2), we get after some manipulations the following explicit relation for the amount adsorbed during any adsorption process:

$$a_a=\frac{a_{j-1}a_{A,j-2}-a_{j-2}a_{A,j-1}}{a_{A,j-2}-a_{A,j-1}}+\frac{a_{j-2}-a_{j-1}}{a_{A,j-2}-a_{A,j-1}}\,a_A=c_1+c_2a_A \quad (21)$$

where constants c_1 and c_2 are defined in Eq. 21. Introducing $a_{A,j-2}=a_{j-2}=a^U$ and $a_{A,j-1}=a_{j-1}=a^L$, we get $a_a=a_A$ for the primary adsorption, and introducing $a_{j-1}=a_{D,j-1}$ and $a_{A,j-1}>a^L$, we obtain the expression Eq. 12 for the secondary adsorption commencing on the primary desorption curve. Similarly, the explicit relation Eq. 21 can be used for the prediction of any adsorption process under isothermal conditions, neglecting the influence of the surface adsorption.

The general theoretical solution Eqs. 19 and 20 for the fraction of pores filled, S_d, can be rewritten to obtain the theoretical amount adsorbed, a_d^t, in the same manner as done for the secondary desorption in Eq. 10. The resulting implicit function G relating the theoretical amount adsorbed, a_d^t, and the relative pressure, x, can be expressed in the general form:

$$G(a_d^t, x)=0 \quad (22)$$

There exist two main complications in using Eq. 22 for the prediction of any desorption process. First and more important, the theoretical relations, Eqs. 19 and 20, or their combined form, Eq. 22, predict the theoretical adsorbed amount a_d^t, which is higher than the real, experimentally observed adsorbed amount, a_d^r (superscript r stands for *real*). This fact was already discussed above. In our previous work (Rajniak and Yang, 1993), we proposed to compute the real amount adsorbed via the empirical relation:

$$a_d^r=a_d^t-\kappa\ln\frac{x^\mu}{x} \quad (23)$$

where the empirical coefficient κ can be evaluated from the shape of the primary desorption isotherm at the upper limiting point (U) of the main hysteresis loop or can be evaluated simultaneously with other adjustable parameters by nonlinear regression (Rajniak and Yang, 1993). The empirical relation (Eq. 23) was originally proposed by Mason (1988) to correct for deviations between the experimental and theoretical (based on the percolation theory for infinite medium) primary desorption curves assuming the dominant role of liquid decompression during desorption. Parlar and Yortsos (1989) showed that the deviations can likewise be explained by heterogeneous nucleation. They expected that at any pressure level, a fraction f_q of the sites (or f_p of the bonds) is allowed to undergo a liquid-to-vapor transition via heterogeneous nucleation. The nucleation fraction was held constant or allowed to increase during the progress of desorption, according to

$$f_q=\exp(-\kappa x) \quad (24a)$$

Parlar and Yortsos (1988) noted that the presence of small amounts of vapor trapped in the porous sample at the termination of primary adsorption would change the behavior of (nominally) primary desorption appreciably. Such vapor occupied pores act as source sites. Then, at the onset of primary desorption at point U, we have $1>q^u\gg 0$ and $1>p^u\gg 0$, and the primary desorption isotherm will follow the secondary desorption curve as computed from Eqs. 3 and 4 for $q_j=q^u<1$ and $p_j=p^u<1$. Such primary desorption curves show behavior similar to that obtained during primary desorption for $p_j=q_j=1$ but for the network of a finite size (Wall and Brown, 1981; Liu et al., 1993). Moreover, Liu et al. (1993) and Ball and Evans (1989) stressed also the importance of a single-pore contribution to hysteresis. They have expected that when few of the pores have access to the vapor phase, the network effect dominates. When many pores have access to the vapor phase, the network effect is less important and the single pore contribution becomes important. On the basis of the observations mentioned above, one can propose another empirical correction function:

$$f_q=1-\exp[-\kappa(x-x^L)] \quad (24b)$$

In the limits for $x=x^U$, we get $f_q>0$, $q=1-f_q<1$, and for $x=x^L$, we obtain $f_q=0$, $q=0$. The relative importance between the single-pore vs. network effect and nucleation vs. decompression contributions to the adsorption-desorption hysteresis-dependent behavior will vary from one sorption system to another and can also influence the choice of a correction function as described above.

By introducing the correction, Eqs. 24a or 24b, into the theoretical relation, Eq. 22, we obtain the following implicit

relation that relates the real amount adsorbed during desorption, a_d^r, and the relative pressure x:

$$F(a_d^r, x) = 0 \tag{25}$$

A second complication follows from the inconvenient form of the implicit expressions (Eq. 22 or 25). Different approaches can be employed to calculate the explicit function:

$$a_d^r = \phi(x) \tag{26}$$

and its derivatives with respect to x (which are necessary, for example, in simulation of diffusion dependent processes.)

The first approach is by the use of the implicit function theorem to be applied to Eq. 25. Suppose F is a continuously differentiable function with respect to a_d^r and x, and $\partial F/\partial a_d^r$ exists, by using the total differential of F:

$$\frac{dF}{dx} = 0 \tag{27}$$

we get

$$\frac{\partial F}{\partial a_d^r}\frac{d a_d^r}{d x} = -\frac{\partial F}{\partial x} \tag{28}$$

which can be used for computation of the first derivative da_d^r/dx. For the evaluation of the second derivative $d^2 a_d^r/dx^2$, the corresponding relation is:

$$\frac{\partial^2 F}{\partial x^2} + 2\frac{\partial^2 F}{\partial x\, \partial a_d^r}\frac{da_d^r}{dx} + \frac{\partial^2 F}{(\partial a_d^r)^2}\left(\frac{da_d^r}{dx}\right)^2 + \frac{\partial F}{\partial a_d^r}\frac{d^2 a_d^r}{d x^2} = 0 \tag{29}$$

The second approach for the approximate evaluation of the explicit function Eq. 26 is based on the assumption that all desorption curves can be described by the same mathematical form of isotherms (Rajniak and Yank, 1993), such as Dubinin-Astakhov type. For the primary desorption isotherm,

$$a_D^r = a^L + a_{mD}\exp\left[-\left(K_D \ln\frac{1}{x - x^L}\right)^{n_D}\right] \tag{30}$$

and for higher-order desorption isotherms:

$$a_d^r = a_{j-1} + a_{mj}\exp\left[-\left(K_j \ln\frac{1}{x - x_{j-1}}\right)^{n_D}\right] \tag{31}$$

The parameters a_{mj} and K_j of the desorption isotherm starting at point $j = \{x_j, a_j\}$ can then be calculated using the ratio of the slopes of the desorption isotherm and of the preceding adsorption isotherm at the onset of desorption, as stipulated by the pore blocking theory. For the ratio of the slopes, a simple general expression can be derived from Eqs. 18-20 and 23:

$$\frac{(da_d^r/dx)_{x=x_j}}{(da_a/dx)_{x=x_j}} = \frac{(q_j - q_{j-1})(q_{j-2} - q_j)}{(q_{j-2} - q_{j-1})(q_j^{1/C} - q_{j-1}^{1/C})q_j^{1-1/C}} + \frac{\kappa/x_j}{c_2(da_A/dx)_{x=x_j}} = E_j \tag{32}$$

The parameters of the primary desorption isotherm a_{mD}, K_D and n_D, and of the primary adsorption isotherms a_{mA1}, K_{A1}, a_{mA2}, K_{A2}, are evaluated by nonlinear regression analysis of the experimental data. Exponent n_D is expected to be constant for all desorption isotherms. E_j in Eq. 32 can be evaluated from the known history of the sorption process and the value of connectivity C and the correction parameter κ. Equation 32 expresses the first condition which must be satisfied for the jth secondary desorption isotherm starting from point j. The second condition follows for the intersection of the adsorption curve and the subsequent desorption curve at point j:

$$a_a = a_d^r \tag{33}$$

Expressing a_a using Eqs. 21 and 1b and a_d using Eq. 31, we get after some manipulations the following explicit expressions for the calculation of parameters a_{mj} and K_j in Eq. 31:

$$K_j = \left(\frac{A_j}{B_j C_j}\right)^{1/n_D}; \quad a_{mj} = \frac{C_j}{\exp[-(K_j D_j)^{n_D}]} \tag{34}$$

where

$$B_j = n_D D_j^{n_D - 1}\frac{1}{x_j - x_{j-1}}; \quad C_j = a_j - a_{j-1}; \quad D_j = \ln\frac{1}{x_j - x_{j-1}}$$

$$A_j = \frac{2}{x_j}\left(\ln\frac{1}{x_j}\right)E_j\left\{a_{mA1}\exp\left[-\left(K_{A1}\ln\frac{1}{x_j}\right)^2\right]K_{A1}^2 + a_{mA2}\exp\left[-\left(K_{A2}\ln\frac{1}{x_j}\right)^2\right]K_{A2}^2\right\}$$

Obviously, other approximation functions for the desorption isotherms can be chosen and more elaborate approximation procedures (based on information at more points and with more adjustable parameters) can be developed. However, to obtain the generally valid description of the desorption processes the procedure using the implicit function theorem, Eqs. 27-29, can be used.

Experimental Studies

The equilibrium adsorption-desorption cycles were measured for water vapor on a standard commercial desiccant, regular-density silica gel, Davison Grade H, at 25°C using a Mettler TA 2000C thermogravimetric analyzer. High purity helium was used as the inert carrier gas and for regeneration. The flow system and the experimental procedure were the same as those described elsewhere (Rajniak and Yang, 1993). The weight of the sample after activation was 62.2 mg.

The sensitivity of the microbalance was 10^{-5} g. The temperature was thermostatted to 25 ± 0.3°C. The fluctuations of the barometric pressure as well as temperature were included in calculating the saturation pressure and the resulting relative pressure.

The BET surface area of the silica gel was 767 m^2/g and the pore volume was 0.398 cm^3/g. The N_2 (77 K) adsorption and desorption isotherm were nearly identical with those reported by Mikhail et al. (1968), with a silica gel sample also from Davison. Based on the isotherms, they obtained a narrow pore size distribution, ranged from approximately 12 to 24 Å.

Table 1. Cyclic Equilibrium Adsorption Data for Water Vapor on Silica Gel at 25°C*

Point	x	a	Point	x	a	Point	x	a
1	0.360	0.203	26	0.686	0.320	51	0.360	0.195
2	0.408	0.230	27	0.743	0.328	52	0.408	0.219
3	0.473	0.254	28	0.609	0.315	53	0.473	0.252
4	0.408	0.239	29	0.546	0.307	54	0.408	0.232
5	0.360	0.222	30	0.473	0.296	55	0.360	0.215
6	0.408	0.232	31	0.546	0.303	56	0.336	0.205
7	0.466	0.252	32	0.607	0.310	57	0.304	0.152
8	0.546	0.286	33	0.743	0.330	58	0.282	0.148
9	0.607	0.297	34	0.607	0.316	59	0.262	0.131
10	0.546	0.288	35	0.544	0.307	60	0.607	0.298
11	0.470	0.278	36	0.473	0.297	61	0.360	0.250
12	0.360	0.254	37	0.360	0.270	62	0.607	0.299
13	0.466	0.272	38	0.473	0.291	63	0.546	0.291
14	0.546	0.283	39	0.544	0.302	64	0.466	0.280
15	0.607	0.296	40	0.606	0.313	65	0.408	0.273
16	0.686	0.318	41	0.635	0.316	66	0.360	0.256
17	0.743	0.328	42	0.606	0.315	67	0.408	0.264
18	0.686	0.324	43	0.544	0.306	68	0.466	0.271
19	0.607	0.313	44	0.472	0.296	69	0.546	0.289
20	0.546	0.306	45	0.360	0.276	70	0.466	0.276
21	0.473	0.295	46	0.000	0.002	71	0.408	0.267
22	0.360	0.277	47	0.262	0.135	72	0.360	0.254
23	0.473	0.292	48	0.282	0.153	73	0.546	0.291
24	0.546	0.302	49	0.304	0.158	74	0.360	0.252
25	0.607	0.314	50	0.330	0.182	75	0.546	0.291

* The amount adsorbed is a in g/g, and x in the relative pressure.

Successive adsorptions and desorptions were conducted at 25°C by changing the composition of the adsorptive and allowing adequate time to establish equilibrium. The experimental results are given sequentially in Table 1. The experimental points 1-15 represent cycle type C2, the points 16-33 are for cycle C3, the points 34-45 represent cycle C4, the points 46-59 are for cycle C1 and the points 60-75 represent cycle C5.

The adsorption properties of the desiccant silica gels are remarkably uniform and reproducible. The available literature data on water vapor adsorption on desiccant silica gels of different grades and from different sources, published in eight papers dating from 1945, were correlated by van den Bulck (1989). The results showed that the adsorption properties were very similar among the large set of data. Moreover, our data shown in Table 1 agreed surprisingly well with van den Bulck's correlation (based on the literature data). The maximum deviation between our data and van den Bulck's correlation was 2.3%.

Results and Discussion

First, the experimental equilibrium data originally reported in our recent article (Rajniak and Yang, 1993) were reanalyzed by using the 2-site Dubinin-Radushkevich isotherm (Eq. 1b) for the primary adsorption data and the Dubinin-Astakhov isotherm (Eqs. 30 and 31) for the primary and secondary desorption data. The regression procedure was the same as that reported in Rajniak and Yang (1993). A sequential evaluation procedure proposed in that work was used to find the parameters of primary adsorption and primary desorption isotherms and the position of their intersections. The values of the empirical constant κ defined by Eq. 23 and the value of connectivity C were calculated from the shape of the primary desorption isotherm at the onset of primary desorption (at the upper closure point) and at the desorption threshold, respectively (Rajniak and Yang, 1993; Mason, 1988). It was also shown earlier (Rajniak and Yang, 1993) that this simple sequential evaluation procedure may be improved, if the secondary desorption data are also used and all parameters are evaluated simultaneously by nonlinear regression. The parameters obtained in this manner are given in Table 2. Significant improvement of the data fit was indeed achieved comparing to the best fit (DA relations for primary adsorption, primary and secondary desorption) obtained earlier (Rajniak and Yang, 1993). The total sum of squares expressed by:

$$SS = \sum_{j=1}^{N} (a_{cal} - a_{exp})_j^2$$

decreased from 6.642×10^{-3} to 4.912×10^{-3}.

Table 2. Parameters of Sorption Isotherms

Primary Ads. DR2 Eq. (Eq. 1b)	Primary Desorp. DA Eq. (Eq. 30)	Limiting Points of Hysteresis Loop
$a_{mal} = 0.2785$	$a_{mD} = 0.1703$	$x^L = 0.3124$
$K_{A1} = 0.8611$	$K_D = 0.1854$	$a^L = 0.1687$**
$a_{mA2} = 0.0679$	$n_D = 1.2289$	$x^U = 0.6915$
$K_{A2} = 0.1151$	$\kappa = 0.0423$*	$a^U = 0.3196$**
	$C = 3.3041$*	

* κ and C are calculated separately from the primary desorption isotherm.
** a^L and a^U are calculated using Eq. 1b.

Another evaluation procedure may be performed in which the desorption curves are described by the theoretical relation, Eqs. 2-4, together with any empirical correction function (Eqs. 23 or 24a or 24b). Two adjustable parameters, κ and C (and x^U eventually, for uncertain position of the upper closure point of the hysteresis loop), obtained in such a manner are in principle similar to those obtained by the method proposed by Liu et al. (1993), in which the connectivity C and the network size, L, are determined from an analysis of the desorption boundary curve.

However, the advantage of our method (Rajniak and Yang, 1993) is that neither the pore size distribution function, nor connectivity or extensive Monte Carlo simulations (as used by Liu et al., 1993) are needed for the evaluation and prediction of primary and secondary desorption isotherms (the value of connectivity is important only for the prediction of the higher-order desorption curves as described by Eq. 19). Various simple correction functions (Eqs. 23 and 24) can be easily incorporated into the model to fit experimental data for various sorption systems.

The experimental cycles from Table 1 and some selected experimental data from our previous work (Rajniak and Yang, 1993) were predicted using Eqs. 21, 30 and 31 with the parameters listed in Table 2.

The experimental data for the equilibrium cycles of type C1 are shown in Figure 8, and are compared with theoretical predictions. These type of cycles (primary adsorption and secondary desorption) were already successfully predicted in our earlier work (Rajniak and Yang, 1993), and a slight improvement was achieved here only by using another primary adsorption isotherm (Eq. 1b). As seen from Figure 8, the prediction for the secondary desorption curve starting at a higher relative pressure is better than that for the secondary desorption curve starting at a lower relative pressure; for the latter the amount adsorbed is underpredicted. This observation is similar to the behavior reported by Liu et al. (1993) for the system nitrogen-alumina and can be associated with the increasingly important contribution by the single-pore hysteresis toward lower pressures. Liu et al. (1993) suggest that when few of the pores have access to the vapor phase, the network effect dominates. When many pores have access to the vapor phase, the network effect is less important and the single-pore contribution becomes apparent. In addition, the single-pore contribution toward hysteresis becomes important in a narrow pore size distribution, which is the case here.

The underprediction of the secondary desorption isotherm starting at a lower relative pressure is obvious also from Figure 9, in which the experimental data for cycles C2 are compared with theoretical predictions. As a consequence, the corresponding secondary adsorption branch is also underpredicted, and the final shape of the cycle is narrower as compared to the experimental data.

The experimental data for cycle type C3 are compared with theory in Figure 10. As discussed above, theoretically there exist two types of cycle C3 depending on whether the lower terminal point is above or below the threshold T (shown in Figure 1). If the top of the primary desorption curve represents liquid decompression (Mason, 1988), then reversible behavior would be expected along the top boundary curve (before reaching the desorption threshold). The secondary adsorption isotherm starting from $x = 0.360$ does not retrace the desorption boundary curve. This behavior seems to be, in fact, quite general (see also experimental points 16-33 in Table 1) and the desorption-adsorption process is irreversible below and above the primary desorption threshold (the experimental relative pressure for the threshold position x^T is about 0.33). These experimental facts support the suggestion by Liu et al. (1992) and Neimark (1991), that desorption occurs above the threshold point via surface clusters of vapor-filled pores or desorption from the largest mesopores, emerging directly at the external surface. From this point of view, the assumption of the same

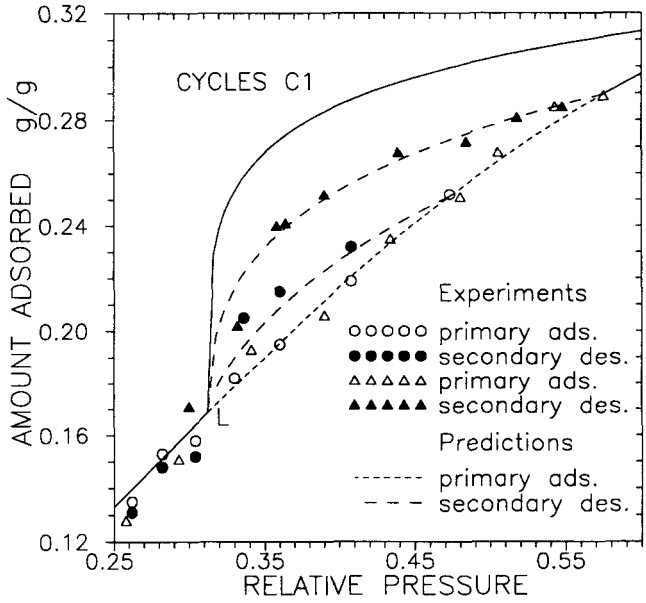

Figure 8. Experimental data on equilibrium cycles C1 compared with theoretical predictions.

All data are for H_2O-Silica Gel at 25°C.

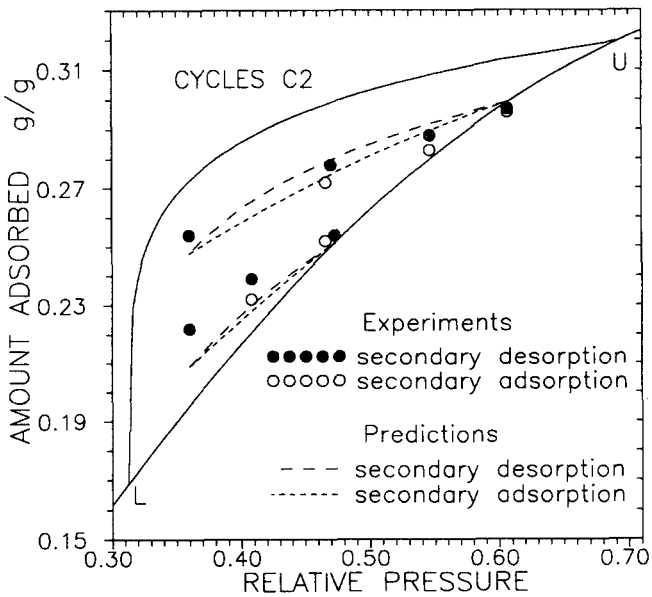

Figure 9. Experimental data on equilibrium cycles C2 compared with theoretical predictions.

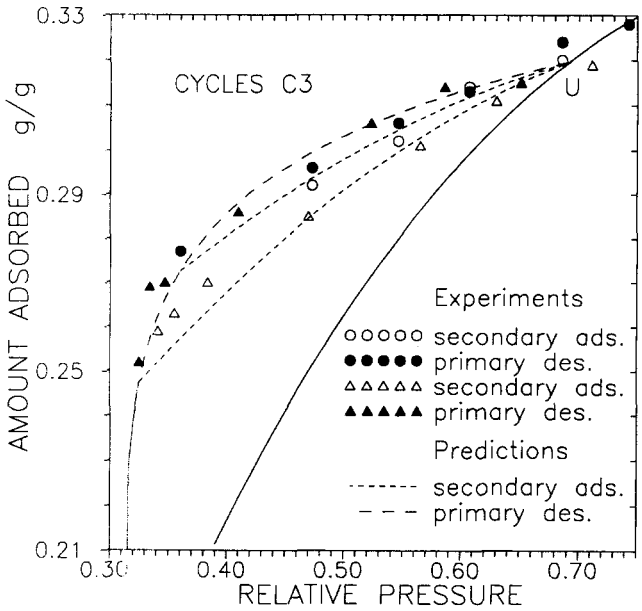

Figure 10. Experimental data on equilibrium cycles C3 compared with theoretical predictions.

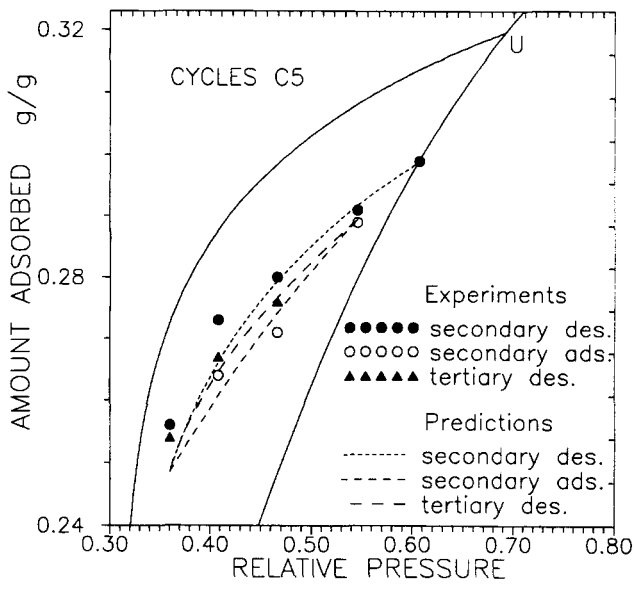

Figure 12. Experimental data on equilibrium cycles C5 compared with theoretical predictions.

mechanism for the desorption below or above the percolation (desorption) threshold, included in the same general prediction seems to be reasonable.

In Figure 11, the equilibrium cycle type C4 is verified. The experimental verification of this cycle type is most difficult, because of very fine differences between the adsorbed amounts during secondary adsorption and desorption processes (note the fine scale used in Figure 11). Theoretical predictions agree qualitatively with the experiments, but again the predicted equilibrium path is narrower than the experimental data. From this point of view the employment of the empirical correction relation (Eq. 23) predicting too steep desorption branches of

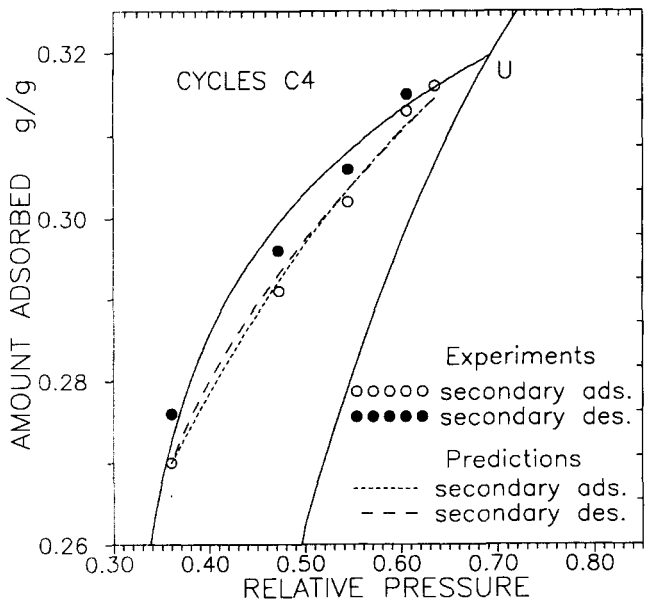

Figure 11. Experimental data on equilibrium cycles C4 compared with theoretical predictions.

the cycles inside the main hysteresis loop should be further studied. The underprediction of the adsorbed amounts during the higher-order desorption processes can be associated again with the increasing role of the single-pore hysteresis discussed recently by Liu et al. (1993), and another correction function, for example, Eq. 24b, can be tested with the experimental data.

The observations described above are also valid for comparisons shown in Figure 12 for cycle C5. The secondary desorption curve is again underpredicted and the whole computed cyclic path is narrower than the experimental results. However, the existence of such a cycle type is experimentally verified and the experimental tertiary desorption lies between the two secondary curves, as shown in Figure 12.

The comparison of the theory with the experimental data for water on silica gel thus shows general agreement, but also reveals some systematic deviations, which cannot be explained only by experimental errors. The presence of the single-pore hysteresis seems to be the possible explanation for the underprediction of the higher-order desorption curves. Indeed, the discrepancies may be a source of information for a better understanding of the sorption process.

However, a main contribution of the present work was to show that multiple cyclic equilibrium paths can exist between two relative pressures (if both lie between the closure points of the main hysteresis loop), depending on the history of the process. The existence of the multiplicity illustrated in (theoretically) Figure 4 is verified experimentally and is shown in Figures 9, 11, and 12. The practical importance of the existence of the various cyclic paths is evident from a comparison of the amounts adsorbed at the two limiting points of the cycle C2 (Figure 9) and at the limiting points of the cycle C4 (Figure 11). Both cycles operated between the same relative pressures $x_1 = 0.360$ and $x_2 = 0.607$, but the amounts adsorbed differ significantly (compare points 12, 15 and 42, 45 in Table 1), $a_1 = 0.254$ vs. $a_1 = 0.276$ and $a_2 = 0.296$ vs. $a_2 = 0.315$. Thus, the amounts adsorbed at the limiting points of the cycle are 7-9% lower for cycle C2 starting from the clean particle, than

for cycle C4 starting from a saturated particle. This multiplicity will have a significant consequence in the performance of industrial adsorbers.

Summary

The hysteresis-dependent adsorption-desorption equilibrium cycles were measured for the system water vapor-silica gel at 25°C. A classification of the equilibrium cycles depending on the positions of the limiting pressures is given. The predictive model recently proposed for the primary and secondary processes (Rajniak and Yang, 1993) is extended for higher-order processes and all possible equilibrium cycles starting from various points inside and outside the main hysteresis loop. For this purpose the general predictive relations for the isothermal processes are derived. It is shown that an infinite number of different equilibrium cycles operating between two relative pressures inside the main hysteresis loop can exist depending on the history of the cyclic process: the cycle path is memory-dependent.

The same procedure is proposed for the prediction of the secondary adsorption processes starting from any point on the primary desorption isotherm (below and above the percolation threshold). This assumption is supported experimentally by the observation of the irreversible behavior of the equilibrium cycle C3 also below the desorption threshold, which can be explained via the formation of surface clusters of vapor filled pores during the primary desorption process.

The theoretical relations predict well the equilibrium cycles measured experimentally.

Acknowledgment

This work was supported by the NSF under Grant CTS-9212279 and in part by the Donors to the Petroleum Research Fund, administered by the American Chemical Society.

Notation

a = amount adsorbed (g/g)
a_m = parameter of isotherm
b = parameter of Kelvin equation, Eq. 7
C = connectivity
$f(r)$ = bond radius distribution function
$g(r)$ = site radius distribution function
K = parameter of isotherm
n = parameter of isotherm
p = bond filling probability, Eq. 5
P = absolute pressure
P_o = saturation pressure
q = site filling probability, Eq. 6
r = bond or site radius
R = gas constant
S = fraction of pores filled, Eq. 9
T = absolute temperature
u = probability that a bond is connected to the vapor during desorption
x = relative pressure, P/P_o

Greek letters

κ = empirical constant, Eq. 11

Subscripts

a = adsorption
A = primary adsorption
d = desorption
D = primary desorption
S = starting point
SA = secondary adsorption
SD = secondary desorption

Superscripts

L = lower closure point of main hysteresis loop
r = real
t = theoretical
T = threshold
U = upper closure point of main hysteresis loop

Literature Cited

Ball, P. C., and R. Evans, "Temperature Dependence of Gas Adsorption on a Mesoporous Solid: Capillary Criticality and Hysteresis," *Langmuir*, **5**, 714 (1989).

Everett, D. H., "Adsorption Hysteresis," *The Solid-Gas Interface*, Vol. 2, E. A. Floor, ed., Marcel Dekker, New York, p. 1055 (1967).

Gregg, S. J., and K. S. W. Sing, *Adsorption, Surface Area and Porosity*, 2nd ed., Academic Press, London (1982).

Liu, H., L. Zhang, and N. A. Seaton, "Determination of the Connectivity from Nitrogen Sorption Measurements: II. Generalisation," *Chem. Eng. Sci.*, **47**, 4393 (1992).

Liu, H., L. Zhang, and N. A. Seaton, "Analysis of Sorption Hysteresis in Microporous Solids Using a Pore Network Model," *J. Coll. Interf. Sci.*, **156**, 285 (1993).

Mason, G., "A Model of Adsorption-Desorption Hysteresis in which Hysteresis is Primarily Developed by the Interconnections in a Network of Pores," *Proc. Roy. Soc. Lond.*, **A390**, 47 (1983).

Mason, G., "Determination of the Pore-Size Distribution and Pore-Space Interconnectivity of Vycor Porous Glass from Adsorption-Desorption Hysteresis Capillary Condensation Isotherms," *Proc. Roy. Soc. Lond.*, **A415**, 453 (1988).

Mayagoitia, V., F. Rojas, and I. Kornhauser, "Domain Complexions in Capillary Condensation, Part 1.—The Ascending Boundary Curve," *J. Chem. Soc., Faraday Trans. 1*, **84**, 785 (1988a).

Mayagoitia, V., B. Gilot, F. Rojas, and I. Kornhauser, "Domain Complexions in Capillary Condensation: 2. Descending Boundary Curve," *J. Chem. Soc., Faraday Trans. 1*, **84**, 801 (1988b).

Mikhail, R. S., S. Brunauer, and E. E. Bodor, "Investigations of a Complete Pore Structure Analysis: I. Analysis of Micropores," *J. Colloid Interf. Sci.*, **26**, 45 (1968).

Neimark, A. V., "A Percolation Theory of Capillary Hysteresis Phenomena and its Application for Characterization of Porous Solids," *Characterization of Porous Solids*, F. Rodriguez-Reinoso, J. Rouquerol, and K. S. W. Sing, eds., Elsevier, Amsterdam, p. 67 (1991).

Park, I., and K. S. Knaebel, "Adsorption Breakthrough Behavior: Unusual Effects and Possible Causes," *AIChE J.*, **38**, 660 (1992).

Parlar, M., and Y. C. Yortsos, "Percolation Theory of Vapor Adsorption-Desorption Processes in Porous Materials," *J. Coll. Interf. Sci.*, **124**, 162 (1988).

Parlar, M., and Y. C. Yortsos, "Nucleation and Pore Geometry Effects in Capillary Desorption Processes in Porous Media," *J. Coll. Interf. Sci.*, **132**, 425 (1989).

Rajniak, P., and R. T. Yang, "A Simple Model and Experiments for Adsorption-Desorption Hysteresis: Water Vapor on Silica Gel," *AIChE J.*, **39**, 774 (1993).

Ritter, J. A., and R. T. Yang, "Equilibrium Theory for Hysteresis-Dependent Fixed-Bed Desorption," *Chem. Eng. Sci.*, **46**, 563 (1991).

Seaton, N. A., "Determination of the Connectivity of Porous Solids from Nitrogen Sorption Measurements," *Chem. Eng. Sci.*, **46**, 1895 (1991).

van Bemmelen, J. M., "Die Absorption. Das Wasser in den Kolloiden, besonders in dem Gel der Kieslsaure," *Z. Annorg. Allgem. Chem.*, **13**, 231 (1897).

Van den Bulck, E., "Isotherm Correlation for Water Vapor on Regular-Density Silica Gel," *Chem. Eng. Sci.*, **45**, 1425 (1990).

Yang, R. T., *Gas Separation by Adsorption Processes*, Butterworth, Boston (1987).

Manuscript received June 11, 1993, and revision received Sept. 14, 1994.